УДК 621.373.8

FIBER LASER DRIVEN THREE-MICRON SOURCE DEVELOPMENT BASED ON DIFFERENCE FREQUENCY GENERATION

© **J. R. Taylor**

Femtosecond Optics Group, Physics Department, Imperial College London, London SW7 2BW, UK
E-mail: jr.taylor@ic.ac.uk

We review our development of wavelength tuneable, high average power, picosecond-pulse, mid-infrared sources in the three micron widow for proposed application in tissue ablation studies and with the objective of source simplification and exploring the potential of all-fiber integration. Initial systems were based on difference frequency generation (DFG) of two synchronous master oscillator power fiber amplifier (MOPFA) schemes. The generated idler was tuneable over the range 3.28–3.45 μm, delivering greater than 3 W of average power, with a maximum pump to total DFG power conversion efficiency of 78 %. By simplifying the seed sources through synchronised in-line modulation of cw diode laser sources, more than 6 W was generated 3.31–3.48 μm with similar efficiency and with near diffraction limited beam quality ($M^2 = 1.4$). In an improved and significantly simplified experimental configuration a source emitting around 3 μm was developed employing a novel $\chi^{(3)}/\chi^{(2)}$ cascaded nonlinear conversion architecture. Picosecond pulses from a 1.064 μm mode-locked Yb:fiber pump laser were used to generate 1.65 μm signal pulses through $\chi^{(3)}$ based four-wave mixing in a polarisation preserving photonic crystal fiber (PCF). The output of the PCF was then directly focused into a periodically poled lithium niobate crystal, generating idler radiation around 3 μm, with peak powers of ∼0.5 kW, via $\chi^{(2)}$-based three-wave mixing between the pump and signal pulses.

Keywords: fiber lasers and amplifiers, MOPFA technology, difference frequency generation, parametric amplification, mid infra-red generation.

DOI: 10.15372/AUT20230103

1. Introduction. In recent years, mid-infrared (IR) sources operating in the 3–5 μm spectral region have become ubiquitous tools in both industry and research, finding applications in areas including spectroscopy, materials processing, and defense [1, 2]. Depending on the laser parameters required, a wide choice of sources exists that emit in this portion of the "molecular fingerprint region." These include quantum-cascade (QC) semiconductor lasers [3], Cr/Fe-doped II-VI chalcogenide solid-state lasers [4, 5], and parametric frequency conversion sources [6]. Of the two direct emission routes, QC lasers are available across a wide spectral range (3–25 μm), but power scaling opportunities are limited. In contrast, Cr:ZnSe/S lasers have been demonstrated with output powers >10 W [4], but their gain bands do not extend beyond about 3.1 μm [5]. Fe:ZnSe/S crystals provide gain in the 4–5 μm window, however, they require cryogenic cooling to lase efficiently and demand complex pumping schemes [4]. Similarly, Cr:CdSe/S lasers offer the potential for wide tuning at wavelengths >3 μm, but remain a relatively underdeveloped technology [7, 8]. Alternatively, parametric wavelength conversion offers high average powers, supports large pulse energies, and wide spectral tunability dependent on the combination of pump source and nonlinear crystal [6, 9]. Parametric sources based on a $\chi^{(2)}$ nonlinearity can be realized using distinct architectures: optical parametric oscillators (OPOs), optical parametric amplifiers (OPAs) and optical parametric generators (OPGs). In particular, ytterbium (Yb) fiber laser pumped OPOs are capable of producing multiwatt-level average powers, from the CW to femtosecond regimes, often accompanied by

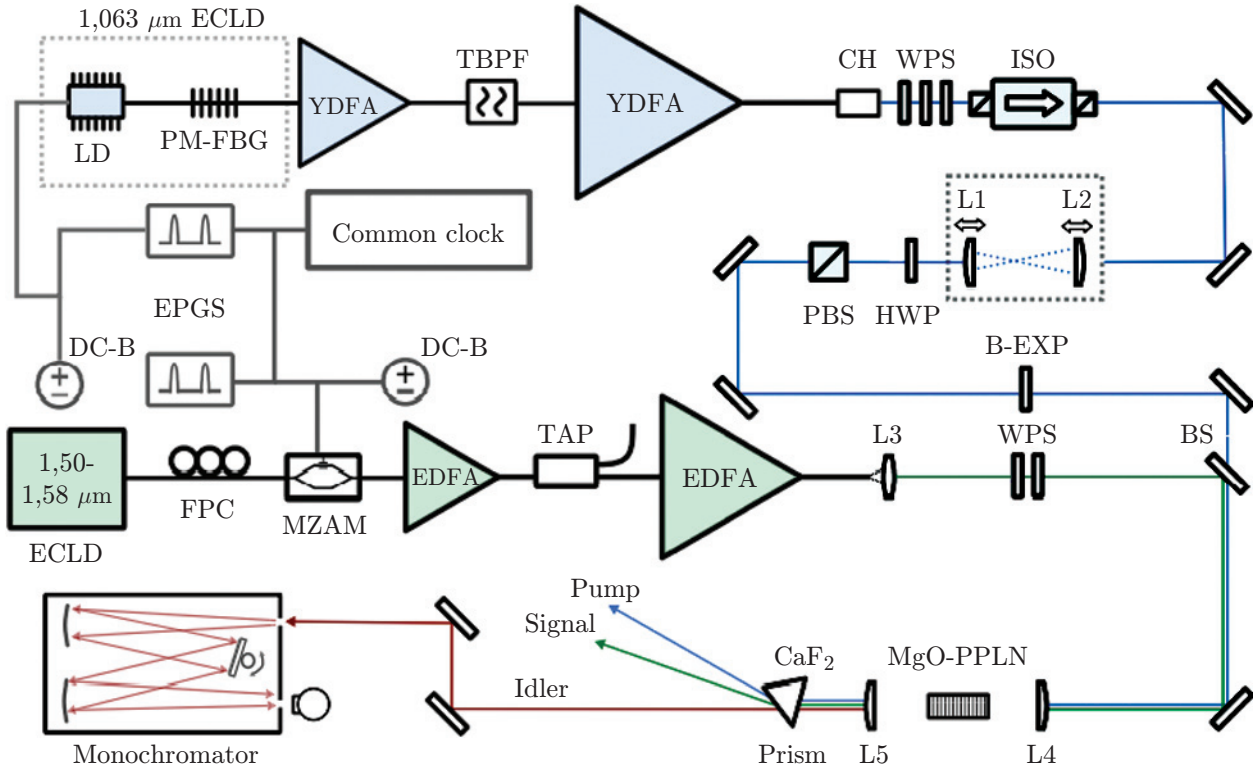

Fig. 1. Experimental configuration for mid-IR difference frequency generation using synchronous fiber lasers (see text)

a wide spectral tuning range [10–12]. However, OPOs have a number of drawbacks inherent in resonant, cavity based systems, including: the need for optics with specialist broadband transmission coatings, precise alignment, and intracavity spectral tuning, while their repetition rate is fixed by the cavity length. OPG, OPA, and difference-frequency generation (DFG), however, provide single-pass amplification, simplifying the optical configuration, and removing the constraint of a resonant cavity. Unfortunately, OPG can result in broad signal and idler linewidths, while the required high pump energies of an unseeded scheme can approach the damage threshold of the crystals used, leading to long-term reliability issues or catastrophic damage. However, for some applications the simplicity of the generation system is particularly attractive, while for some applications broad spectral width of the idler signals may not be problematic, for example in ablation of tissue where extended spectral absorption bands often exist. This is exemplified around 3 μm where pulsed picosecond MIR sources at have vast potential for precise ablation in applications, particularly including surgery. Downconversion techniques used in a single pass architecture (optical parametric amplification (OPA) and difference frequency generation (DFG)) offer significant flexibility in output pulse duration and repetition rate that is not possible in the corresponding cavity-based architecture of the optical parametric oscillator (OPO). In contrast to OPOs which require cavities that can be bulky and vulnerable to external disturbances, the simpler single-pass approaches therefore lend themselves to robust, reliable, and compact devices. Here we describe steps in the development of a simple single pass configuration for applications in ablation with the potential for all-fiber integration.

2. Difference frequency generation using synchronously pulsed fiber lasers. The most obvious and basic approach to generation around 3 μm is to undertake the difference frequency mixing of a Yb (1063 nm) fiber laser and an Er (1550 nm) fiber laser. Employing

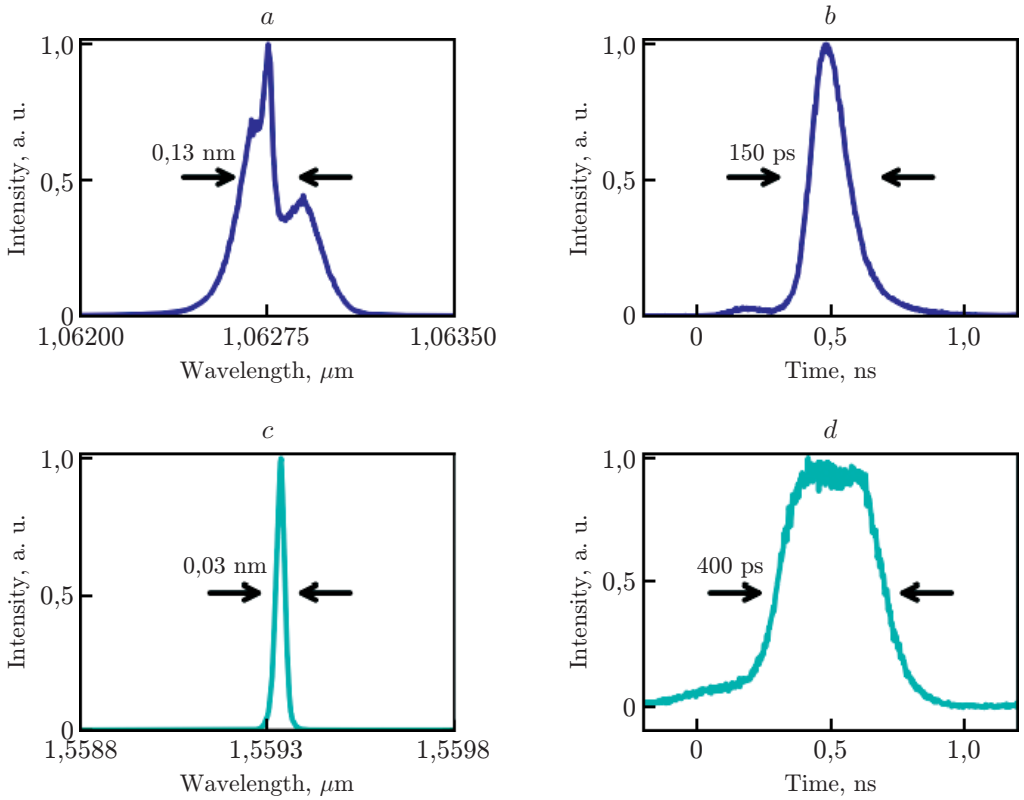

Fig. 2. (a) and (b): Pump; and (c) and (d): signal; spectral and temporal characteristics at MOPFA outputs (23.0 W and 2.1 W, respectively)

pulsed excitation increases the efficiency of the process, however, it does introduce the practical problem of synchronisation. The experimental setup [13] is shown in Fig. 1. The pump arm consisted of an actively mode-locked external cavity laser diode (1.063 μm ECLD), with feedback provided by a polarization-maintaining fiber Bragg grating (PM-FBG), and driven by an electrical pulse generator (EPG). A DC-bias (DC-B) voltage allowed for optimization of the pulse duration and extinction ratio. The 150 ps pulses [Fig. 2(b)] had a repetition rate of 39.945 MHz, half the fundamental cavity frequency of the ECLD. The pulses were then amplified in two Yb-doped fiber amplifiers (YDFAs), with interstage amplified spontaneous emission (ASE) suppression provided by a 1 nm full-width half-maximum (FWHM) tunable bandpass filter (TBP). Due to the use of isotropic gain fiber, polarization control comprising a quarter/half/quarter waveplate combination (WPS) was required to correct for polarization rotation in the amplifier stages. The power level of the Yb-MOPFA after the Faraday isolator (ISO) was ~23 W, with the spectral and temporal characteristics of the pump after amplification shown in Fig. 2(a) and Fig. 2(b), respectively. A beam expander (B-EXP-L1, $f = 50$ mm; L2, $f = 81$ mm) then resized the pump beam for optimal spatial overlap with the signal beam in the nonlinear crystal. Finally, a half-wave plate (HWP) and polarizing beam splitter (PBS) were used to control the pump power delivered to the nonlinear crystal. The signal arm consisted of a tunable ECLD (1500–1580 nm), pulsed by a Mach–Zehnder amplitude modulator (MZAM) driven by a second EPG, producing 400 ps pulses [Fig. 2(d)] at a repetition rate of 39.945 MHz. The two EPGs were synchronized using a common clock. The signal was then amplified in two Er-doped fiber amplifiers (EDFAs), with a 2 % tap-coupler (TAP) to monitor the pulse extinction ratio. The output of the second EDFA was collimated with a lens (L3, $f = 12.5$ mm) chosen to match the spot sizes of the pump and signal beams in the crystal. The Er-MOPFA provided 2.1 W of average power at the output of L3. A quarter/half WPS was used to linearize

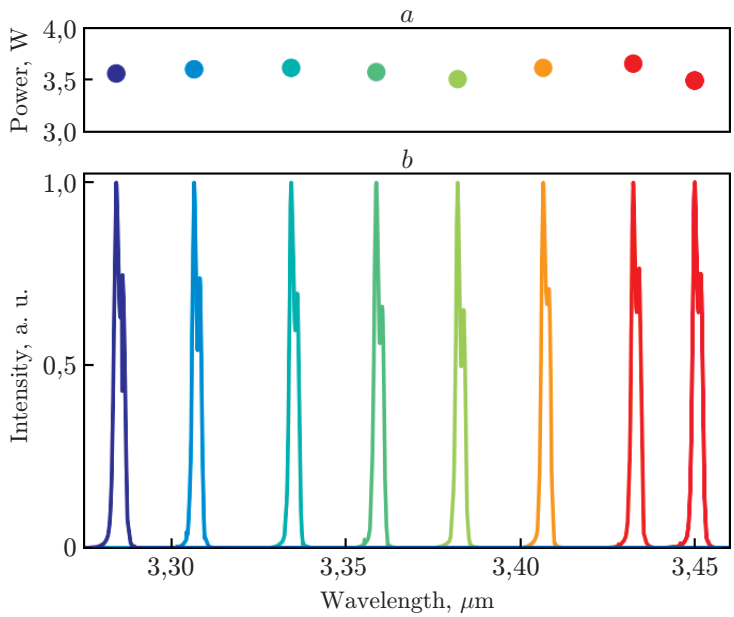

Fig. 3. (a) Maximum idler average powers across tuning range. (b) Idler wavelength tuning through signal wavelength scanning

the output polarization from the non-PM EDFAs. The spectral and temporal characteristics of the signal after amplification are shown in Fig. 2(c) and Fig. 2(d), respectively. The pump and signal were combined using a beam splitter (BS, highly reflective at 1.55 μm and highly transmissive at 1.06 μm). The B-EXP and L3 allowed the ratio of the beam diameters of the pump to signal to be adjusted to 1.06/1.55, ensuring equal focal spot sizes in the center of the crystal. Lens 4 (L4, $f = 150$ mm) was then used to focus the spatially and temporally overlapped pump and signal beams into the MgO:PPLN crystal. The pump beam was focused to a $1/e^2$ beam diameter of 150 μm, measured using a scanning-slit beam profiler. The intensity of the pump at the focal spot in the crystal, at the maximum available pump power, was estimated to be 28 MW/cm^2, well below the 0.1–1 GW/cm^2 damage threshold range — one of the benefits of a synchronously pumped DFG system. The MgO:PPLN crystal was mounted in a copper oven, capable of maintaining crystal temperatures in the range 20−250 ± 0.1 °C. Both the input and output faces of the crystal were antireflection (AR)-coated for pump, signal, and idler wavelengths. The crystal was 40 mm long with an aperture of 1 × 10 mm, and contained five poling periods in the range 29.52–31.52 μm. For the results reported, a track with a period of 29.98 μm was used.

The pump, signal, and generated idler were collimated using lens 5 (L5, $f = 100$ mm, uncoated CaF_2) before being spatially dispersed using an uncoated CaF_2 prism. Initially, a liquid nitrogen-cooled InSb detector was used to record the idler power and optimize the pump/signal overlap, both spatially and temporally in the crystal. The EPGs provide electrical delay control, enabling temporal overlap of the pump and signal pulses. The electrical rather than an optical delay also negated problems associated with beam misalignment when changing the optical path length of the pump relative to the signal. Figure 3(b) shows the generated idler spectra, while tuning the signal wavelength over the range 1.535–1.570 μm, measured using a scanning monochromator. The temperature of the crystal was tuned over the range 130–210 °C to maintain phase-matching. The tuning range of the signal, however, was limited by the gain bandwidth of the Er-MOPFA. Greater than 3.4 W of average idler power was maintained across the full tuning range [Fig. 3(a)]. Excellent agreement was achieved between the experimentally measured signal/idler wavelengths as a function of the phase-matched crystal temperature,

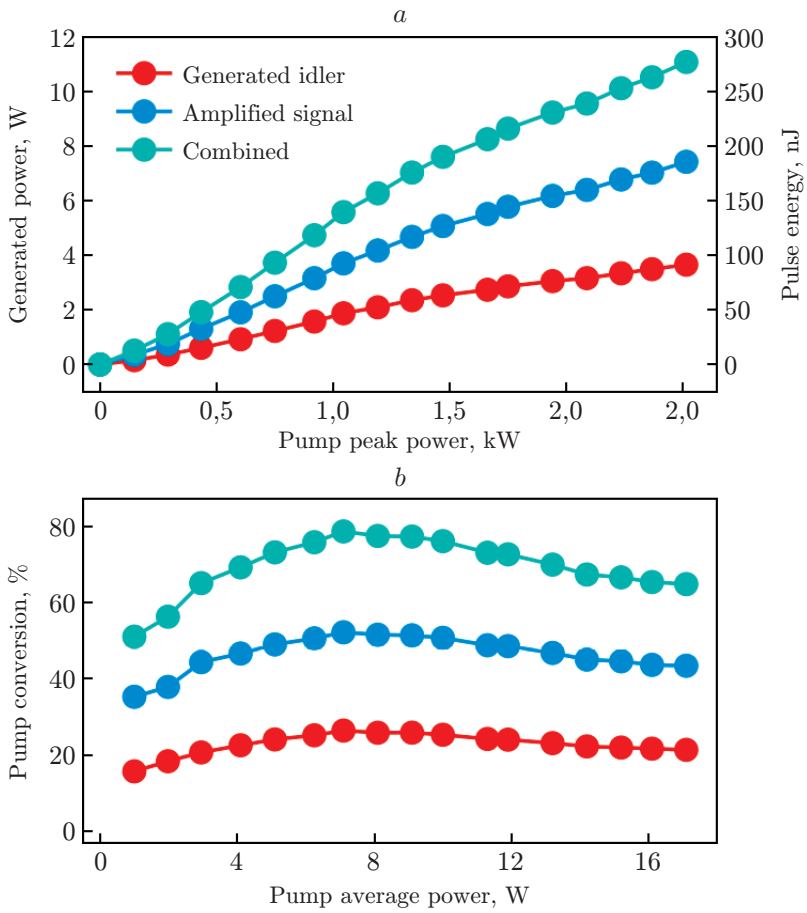

Fig. 4. (a) Signal (blue), idler (orange), and total (signal plus idler-green) powers generated for a given pump average (bottom axis)/ peak-power (top axis), with pulse energy shown on right-hand axis. (b) Signal, idler, and total pump power conversion

compared to the theoretically predicted values. Some spectral structure observed in the idler was directly attributed to spectral structure in the profile of the pump. The idler output power exhibited excellent power stability, with a root-mean-square power deviation of less than 0.4 % over a 90 min period.

The variation of the output powers with pump power is shown in Fig. 4(a), for a pump/signal wavelength of 1.063/1.560 μm. The data represents the average powers generated in the DFG process, with the input signal power (1.87 W) subtracted from the generated signal. A maximum idler power of 3.66 W was obtained at a wavelength of 3.334 μm and a pump power of 17.1 W/2.5 kW (av./pk.). In all the power metrics presented, we considered the loss contribution from optics after the crystal, thus the data represents the power measured directly at the exit face of the crystal.

The corresponding conversion efficiency of the process is shown in Fig. 4(b). We defined pump conversion as the percentage of the total input pump power converted to either the idler, the amplified signal, or the total generated DFG power. The conversion efficiencies reach a maximum of ∼26 % for the idler, ∼52 % for the signal, and ∼78 % for the combined power (amplified signal + idler). Beyond a pump power of 8 W, a roll-off in the conversion efficiency was observed, attributed to back-conversion of the signal and idler power to the pump beam. This was supported by evidence gathered from direct streak camera temporal measurements of the pump pulse, initially showing depletion at intermediate pump power levels and with

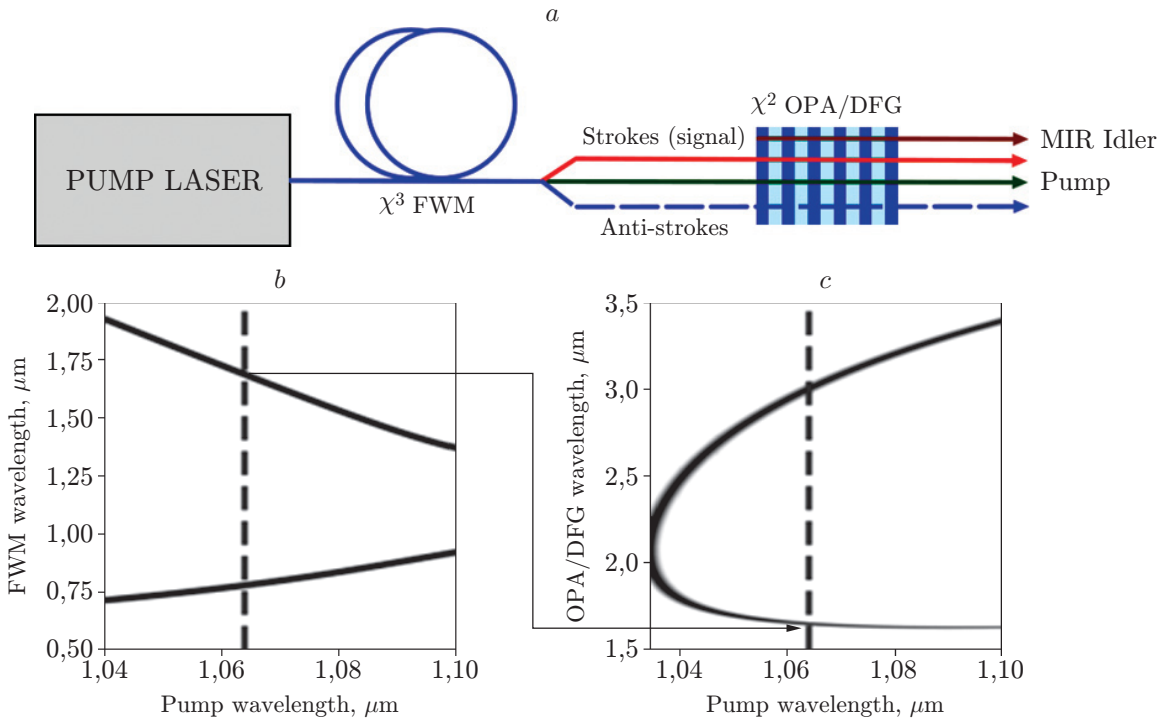

Fig. 5. Schematic of experimental configuration used for MIR generation via cascaded four-wave mixing in fiber with sequential optical parametric amplification/difference frequency generation in a bulk non-linear crystal. (b) The phase matching diagram for FWM in PCF. (c) Phase matching diagram for OPA/DFG in PPLN, with the red arrowed line from (b) to (c) showing how the Stokes component of FWM was used as signal in the DFG process

subsequent recovery of the depleted region at higher pump powers [13].

Although the technique allowed high overall conversion efficiency for the DFG process, the use of a directly modulated semiconductor gain element in an extended cavity configuration as the seed laser severely limits the flexibility of the overall system in terms of pulse width and pulse repetition rate selectivity. Consequently, in an improved experimental setup [14] the seed source for the pump was replaced by a cw operating DFB laser diode at 1.065 μm fiber coupled to an inline electro-optic modulator that allowed selectable pulse durations 0.1–3 ns at repetition rates in the range 1–50 MHz and maximum average pump powers in excess of 25 W at the input to the poled crystal. The signal was similarly provided via a tuneable, cw, external cavity laser diode, fiber coupled and externally modulated by a electro-optic modulator driven synchronously with the pump. The generated idler, tuned from 3.31 μm to 3.48 μm with a conversion efficiency of 24 %, generating in excess of 6W average power in the mid infrared. Despite the relatively attractive operating parameters the source, as a clinical instrument it did not present an attractive proposition, through the necessary use of a dual MOPFA pump scheme, with its associated cost, together with open beam operation and use of bulk optic components necessitated by the need to control the polarisation from non-polarisation preserving amplifiers which led to potential instability in field operation as well as the need for system optimisation by an operator. Consequently, a more compact, fiber integrable source was proposed.

3. Mid-infrared difference frequency generation pumped by a fiber based four-wave mixing source. Here we describe and demonstrate a simple technique to generate synchronised pump and signal pulses for seeding DFG or OPA. We employed four-wave mixing

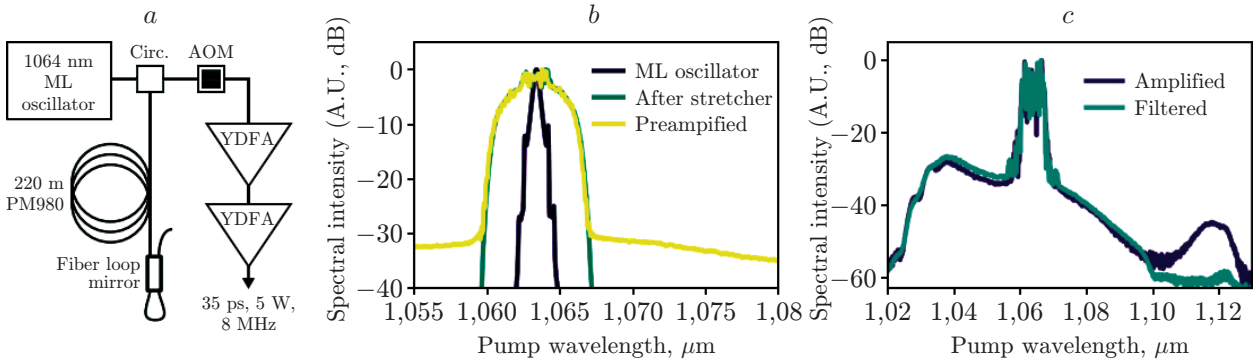

Fig. 6. (a) Yb-master oscillator power fiber amplifier (MOPA) system. ML, mode-locked; Circ., Fiber circulator; AOM, acousto-optic modulator; YDFA, ytterbium-doped fiber amplifier. (b, c) Pump laser spectra at different positions along the MOPA chain

($\chi^{(3)}$) in a photonic crystal fiber (PCF) to produce Stokes (signal) pulses, which were then used as the signal in a conventional $\chi^{(2)}$ three-wave mixing OPA/DFG stage. A schematic of the experimental configuration is shown in Fig. 5. FWM in fiber (in this case a PCF) pumped in the low normal dispersion region generates Stokes and anti-Stokes pulses that can be widely spaced in frequency (>100 THz) from the pump, depending on the dispersion properties of the host fiber and pump wavelength. The Stokes and anti-Stokes pulses generated by FWM in the fiber are overlapped temporally with the remaining pump pulse at the output of the fiber, on the condition that the nonlinear fiber is short compared to the walk-off length due to dispersion. Consequently synchronisation of pump and Stokes signals is automatically assured and by focusing the fiber output directly into an a suitably phase matched $\chi^{(2)}$ nonlinear crystal, difference frequency generation resulting in MIR idler generation is achieved. This removes the need for any beam combination or delay optics, and makes this architecture suitable for full fiber integration. Significant wavelength tuning of the Stokes wavelength produced in the PCF is also possible by altering the dispersion of the PCF [15]. Thus, near arbitrary pairs of pump/Stokes wavelengths can be produced to pump the OPA stage, producing selectable wavelengths throughout the MIR, provided a suitable crystal is available to phasematch the wavelengths of interest.

In the initial demonstration of the technique a picosecond pulsed 1.064 μm Yb-fiber master oscillator power amplifier (MOPA) system was used to pump a length of PCF generating a Stokes wavelength around 1.65 μm via FWM. This was sequentially followed by a periodically poled lithium niobate (PPLN) crystal which was used to phasematch the pump and the Stokes pulses to generate MIR light around 3 μm via DFG. The phase matching diagrams for the FWM and the DFG processes are shown in Fig. 5(b) and (c) respectively.

The MOPA pump system was constructed using polarization-maintaining components and seeded by a 50 MHz mode-locked Yb-fiber oscillator that produced 5 ps pulses. The seed pulses were stretched to 35 ps in a double pass of a 220 m length of polarization maintaining fiber (PM980), enabled through the use of a circulator and fiber loop mirror. A more versatile source would incorporate a cw tuneable semiconductor laser followed by a fiber integrated electro-optic modulator, as described above, in order to produce seed pulses with selectable durations in the range 50 ps — 1 ns. Temporal stretching of the pulses from the seed source was essential in order to promote efficient four-wave mixing in the PCF conversion stage and minimize walk-off between the pump and Stokes signals. An acousto-optic modulator was used to decrease the repetition rate by a factor of 1/6 to approximately 8 MHz and to increase the achievable peak-power of the pump. Two stages of amplification were used achieving an average power

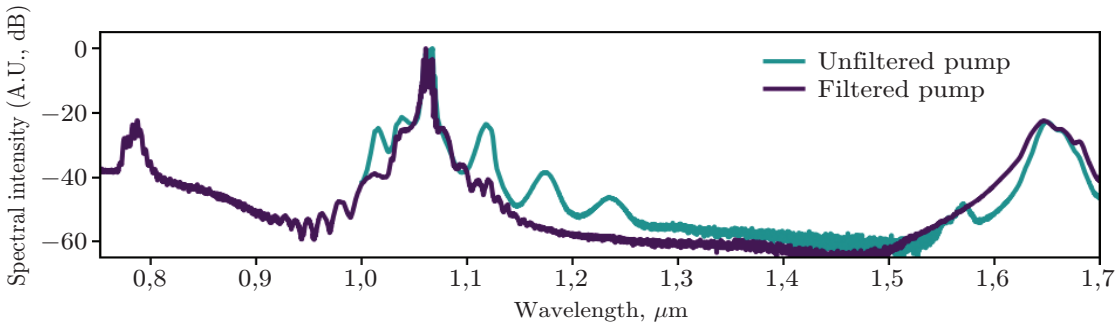

Fig. 7. Output spectrum from PCF, with and without long pass 1100 nm filtering of the pump source to remove Raman scattered light

to 5 W. Residual 976 nm pump power was filtered from the collimated output of the MOPA. An optical isolator was used to prevent backreflections into the system, with a polarizing beam spliter and half wave plate providing power control. A schematic of the MOPFA configuration is shown in figure 6(a). The pump laser spectra at various points along and at the output the MOPA chain are shown in Fig. 6(b-c). The majority of the spectral broadening occured in the stretching fiber, after which the 10 dB spectral width was 5.7 nm. The output spectra after the final stage of amplification remained centered around 1.064 μm with a 10 dB spectral width of 7.1 nm. A final filtering stage was implemented using a long pass dichroic filter with a cut-on wavelength of 1100 nm to remove light around 1120 nm resulting from stimulated Raman scattering in the final amplifier stage, as is shown in Fig. 6(c).

Four wave mixing was carried out in a polarization preserving PCF which had zero dispersion wavelengths of 1.101 μm and 1.103 μm on the fast and slow axes respectively. The corresponding phase-matching diagram for the slow axis of the PCF can be seen in Fig. 5(b). Spectral filtering to remove Raman shifted power in the pump spectrum (Fig. 6(c)), was required before launching the pump into the PCF to prevent the associated losses due to further cascaded Raman shifts. Fig. 7 shows the output spectra of a 0.35 m length of PCF pumped on the slow axes with ∼3 W of coupled pump power, with and without 1100 nm long-pass Raman filtering before the PCF. FWM Stokes and anti-Stokes sidebands were generated in both cases, however without pre-filtering, significant power was transferred to the $n = \pm 1, 2$ Raman shifts ($n \times 13.2$ THz in silica) from the pump.

The Stokes and anti-Stokes sidebands generated by FWM in the PCF depended on the pump polarisation relative to the PCF fast and slow axes. As the pump polarisation was rotated, the two distinct axes were easily identified by the change in generated Stokes wavelength. For intermediate launched pump polarisations which did not align with either axes, the Stokes spectral intensity and spectral width were reduced. When the launched pump polarization state was orientated at 45° to each of the axes of the fiber, sidebands corresponding to both the fast and slow axes were observed. For a given pump axis alignment the peak Stokes wavelength decreased as the coupled pump power increased and significant Stokes spectral broadening occurred, as illustrated in figure 8.

The output of the PCF was focused directly into a PPLN crystal doped with 5 mol.% MgO with a poling period of 31.3 μm, and dimensions $3 \times 3 \times 10$ mm. Using an achromatic lens with focal length 35 mm, a longitudinal offset of 0.8 mm was measured, using a scanning slit beam profiler, between the focus of the pump and Stokes beams due to chromatic aberrations. The greatest MIR idler generation was observed for the shortest focal length focusing lens and consequently the greatest pump and signal intensity in the crystal, however, the crystal oven size physically limited the shortest possible focal length lens to 35 mm. At this focal length, the Rayleigh range of the pump in free-space (approximately 0.7 mm) was significantly shorter

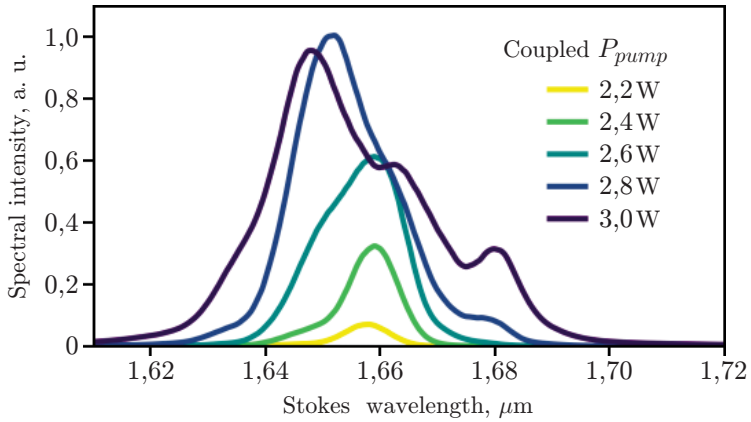

Fig. 8. Variation of the generated Stokes sideband with coupled pump power on the fast axis

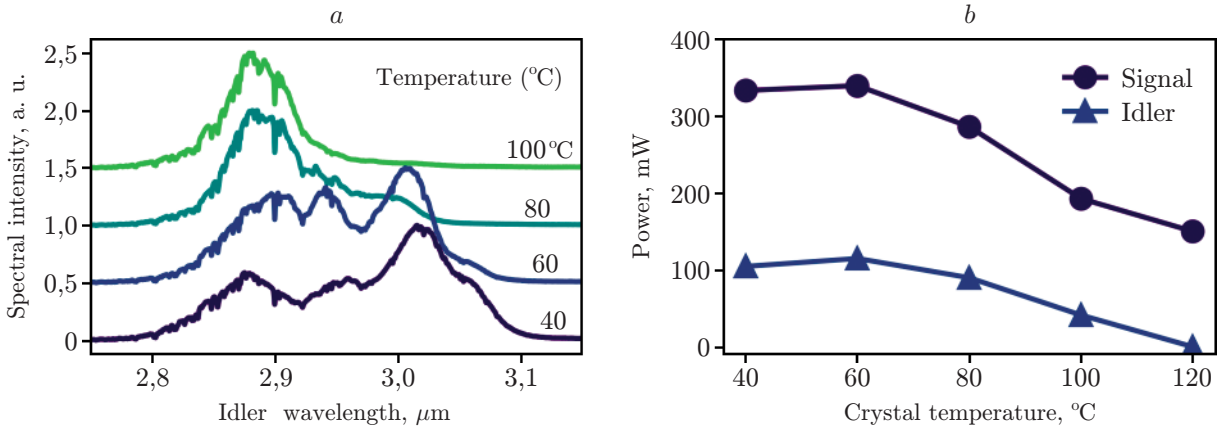

Fig. 9. (a) Idler wavelength tuning with temperature. (b) Idler and amplified signal power tuning with temperature

than the crystal length (10 mm). Tuning the crystal temperature in the range 40−100° resulted in tuning of the idler spectra as shown in Fig. 9(a). The associated variation in the generated idler and amplified signal powers is shown in Fig. 9(b). The phase matched signal wavelength increases with temperature for a fixed pump wavelength. The peak wavelength of the generated idler therefore decreased as the crystal temperature was increased. At a temperature of 120°, the seed signal was no longer phase matched and no idler power was generated, confirming that the FWM Stokes pulses were seeding the MIR generation. A maximum 115 mW of generated idler at around 3 μm together with 189 mW of amplified signal were generated at a crystal temperature of 60°.

4. Conclusions. Although the difference frequency mixing of pulsed Yb- and Er-based MOPFA systems allows the efficient generation of broadly tunable radiation around 3 μm with average and peak powers at the multi watt and kilowatt power levels respectively, the requirement of two pump laser systems together with the use of bulk optics and associated coupling and stability problems makes the source unattractive for wide spread deployment and integration into clinical equipment. Consequently, a simpler solution was successfully investigated through cascading $\chi^{(3)}$ FWM in fiber and sequential $\chi^{(2)}$ DFG in a nonlinear crystal. The simple architecture utilized the inherent spatial and temporal overlap of pulses generated by FWM in fiber to both pump and seed the DFG, requiring only a single pump source. In addition, the configuration has the potential for complete fiber integration including delivery of the generated MIR signals via hollow core photonic crystal fiber. The technique has

been used to generate tuneable MIR light at around 3 μm, with average powers of ∼150 mW and peak power of ∼0.5 kW and has the potential to be significantly power scaled. Even with the specifications reported here, this source is a useful source and wavelength for tissue ablation applications [16]. Development is ongoing to improve the versatility of the seed source and to power scale the overall output as well as operation in different wavelength regions through the incorporation of various PCF structures.

Acknowledgements. The author thanks and acknowledges the extensive contributions of his colleagues in the Femtosecond Optics Group, Mr Ronan Battle, Dr Anita Chandran, Dr. Robbie Murray and Dr Tim Runcorn, throughout the development programme reported and reviewed in this article.

The author also wishes to express his gratitude to the IPG Group of companies for their continued support.

REFERENCES

1. **K. l. Vodopyanov**, Laser-Based Mid-Infrared Sources and Applications, ISBN:9781118301814, Wiley (2020)
2. **F. K. Tittel, D. Richter, and A. Fried**, in Solid-State Mid-Infrared Laser Sources, I. T. Sorokina and K. L. Vodopyanov, eds. (Springer, 2003), pp. 458–529.
3. **Y. Yao, A. J. Hoffman, and C. F. Gmachl**, Nat. Photonics 6, 432 (2012).
4. **S. B. Mirov, V. V. Fedorov, D. Martyshkin, I. S. Moskalev, M. Mirov, and S. Vasilyev**, IEEE J. Sel. Top. Quantum Electron. 21, 292 (2015).
5. **E. Sorokin, S. Naumov, and I. T. Sorokina**, IEEE J. Sel. Top. Quantum Electron. 11, 690 (2005).
6. **A. Godard**, C. R. Phys. 8, 1100 (2007).
7. **E. Sorokin, D. Klimentov, M. P. Frolov, Yu. V. Korostelin, V. I. Kozlovsky, Yu. P. Podmar'kov, Ya. K. Skasyrsky, and I. T. Sorokina**, Appl. Phys. B 117, 1009 (2014).
8. **V. I. Kozlovsky, V. A. Akimov, M. P. Frolov, Yu. V. Korostelin, A. I. Landman, V. P. Martovitsky, V. V. Mislavskii, Yu. P. Podmar'kov, Ya. K. Skasyrsky, and A. A. Voronov**, Phys. Status Solidi B 247, 1553 (2010).
9. **V. Petrov**, IEEE J. Sel. Top. Quantum Electron. 21, 193 (2015).
10. **F. Adler, K. C. Cossel, M. J. Thorpe, I. Hartl, M. E. Fermann, and J. Ye**, Opt. Lett. 34, 1330 (2009).
11. **L. Xu, H.-Y. Chan, S.-U. Alam, D. J. Richardson, and D. P. Shepherd**, Opt. Lett. 40, 3288 (2015).
12. **M. Ebrahim-Zadeh and S. Chaitanya Kumar**, IEEE J. Sel. Top. Quantum Electron. 20, 624 (2014).
13. **R. T. Murray, T. H. Runcorn, E. J. R. Kelleher and J.R. Taylor**, Opt. Lett. 41, 2466 (2016).
14. **R.T. Murray, T.H. Runcorn, S. Guha and J. R. Taylor**, Opt. Express 25, 6421 (2017).
15. **L. Lavoute, J. C. Knight, P. Dupriez, and W. J. Wadsworth**, Opt. Express 18, 16193 (2010).
16. **S. Amini-Nik, D. Kraemer, M. L. Cowan, K. Gunaratne, P. Nadesan, B. A. Alman, B and R. J. D. Miller**, PLOS ONE 5, 1 (2010).

Received 31.10.2022
Revised 02.12.2022
Accepted 02.12.2022